Lawrence Berkeley National Laboratory
Recent Work

Title

Image-Based Cardiac Strain: Progression of Diastolic and Systolic Dysfunction in the
Spontaneously Hypertensive Rat:

Permalink

Authors

Farrar, Genevieve E.
Gullberg, Grant T.
Segars, W. Paul
et al.

Publication Date

2016-08-11

Image-Based Cardiac Strain: Progression of Diastolic and Systolic Dysfunction in the Spontaneously Hypertensive Rat

Genevieve E. Farrar, Grant T. Gullberg, W. Paul Segars, Alexander I. Veress

Genevieve E. Farrar
Department of Mechanical Engineering
University of Washington
Stevens Way, Box 352600
Seattle, WA 98195
gfarrar@uw.edu

Grant T. Gullberg
Life Science Division,
E. O. Lawrence Berkeley National Laboratory
Berkeley, CA 94720
Department of Radiology
University of California San Francisco
San Francisco, CA
gtgullberg@lbl.gov

W. Paul Segars
Duke University,
Department of Radiology
Carl E. Ravin Advanced Imaging Laboratories
Duke University Hock Plaza, Suite 302
2424 Erwin Road
Durham, NC 27705

Alexander I. Veress
Department of Mechanical Engineering
University of Washington
Stevens Way, Box 35260
Seattle, WA 98195
averess@uw.edu

ABSTRACT

Hypertension is a major risk factor for death worldwide. Long-term hypertension causes changes in both diastolic and systolic left ventricular (LV) function, which ultimately lead to heart failure. In this study, image-based strain analysis was used to evaluate the progressive changes LV function (strain) over the lifespan of a commonly used animal model of hypertension. The novelty of the study was that each image dataset was analyzed over the cardiac cycle relative to an in-vivo reference configuration, thereby obtaining separate measures of diastolic and systolic strain, and enabling the assessment of the separate time courses of changes in diastolic and systolic function. The results indicated that decreases in diastolic function may have preceded decreases systolic function.

INTRODUCTION

Hypertension currently affects approximately one third the population in the United States, and represents a major economic burden on the health care system with an estimated annual direct and indirect cost of $50.6 billion (Roger et al. 2012). In hypertension, the left ventricle (LV) must work against increased systemic pressure, which leads to progressive hypertrophic remodeling of the LV characterized by thickened cardiomyocytes and increased collagen ratio (Frohlich et al. 1992). Hypertensive disease leads to changes in both diastolic and systolic function (Hennersdorf and Strauer 2007), and these two aspects of the altered LV function are thought to have different time courses and different underlying mechanisms (Aronow 2006). A detailed understanding of the long-term changes in both diastolic and systolic LV function that occur in hypertension is of great importance to the continued development of mechanics-based treatment approaches.

The spontaneously hypertensive rat (SHR) is the most commonly used animal model for evaluating the long term affects of hypertension induced hypertrophy and heart failure because it closely mimics the physiological and geometric changes associated with hypertension and hypertrophy in man (Bing et al. 2002), and because its relatively short two-year lifespan facilitates longitudinal studies. Changes in global function measures such as ejection fractions (EF) are well documented in the SHR (Bing et al. 1995, Pfeffer et al. 1979). However, EF does not separate diastolic and systolic dysfunction, and does not capture spatial variation in function.

Medical imaging-based strain studies have emerged as effective means of characterizing the local tissue deformation of the LV (Costandi et al. 2007, Feng et al. 2009, Phatak et al. 2009). Another potential advantage of image-based strain measurement, for the specific case of gated cardiac imaging data, is the ability to separate diastolic and systolic strains. By quantifying LV deformation relative to an in-vivo reference configuration, diastolic and systolic strains could be assessed independently.

The 3D strain field of the LV can be determined from clinical imaging data with an existing image registration technique known as Hyperelastic Warping (Veress 2005). Warping uses the differences in image intensity between a template (reference) image data set and a target (deformed) image data set to deform a finite element (FE) representation of the template geometry into alignment with the target geometry, and thus obtains the deformation map between the two states (of the cardiac cycle) in the form of nodal strains (Veress AI 2013, Veress 2005). In previous work, Warping has been applied to:

- SHR microPET images for evaluating LV strains at end-diastole referenced to end-systole (Veress et al. 2008),

- human PET images for evaluating LV strains at end-systole referenced to end-diastole (Veress 2013),

- human cineMRI images for evaluating LV strains at end-systole referenced to end-diastole (Phatak et al. 2009),

- human cineMRI images for evaluating LV strains at end-diastole referenced to end-systole (Veress et al. 2005).

In all prior studies, strain was measured between images at end diastole and end systole, and thus combines both diastolic and systolic function. Warping also has the advantage that it can be applied to a series of image data points representing different points in the cardiac cycle thus allowing for separate evaluation of diastolic and systolic function. The objective of this study was to use warping image registration to determine LV strain distributions based on gated microPET images acquired of 7 SHR and 6 Wistar-Kyoto (WKY) controls at 4 points in time over their lifespans, and assess the long-term changes in myocardial strains associated with hypertensive hypertrophy in the SHR. The novelty of the approach was that each image dataset was analyzed over the cardiac cycle relative to an in-vivo reference image,

which produced separate measurements for diastolic and systolic strains, and enabled the assessment of the separate time courses of changes in diastolic and systolic function.

50

METHODS

Animal Study Design

55   All imaging studies were performed in accordance with Institutional Animal Care and Use

Committee (IACUC) approved protocols from both UCSF and Lawrence Berkeley National Laboratory.

Eight male SHRs and eight male WKY normotensive rats were purchased from Charles River

Laboratories (Wilmington, MA). Imaging began at approximately six months of age and the rats were

imaged throughout their life cycle at separate time points corresponding to 6, 12, 15, 18 and 20 months

60   of age. All rats were freely fed standard Purina rat chow and water. During each time point, every living

rat was imaged using ^{18}F-flurodihydorotenol. The rats were not fasted for the studies.

MicroPET Imaging

Temporal changes in geometry and deformation were documented through multiple image

65   acquisitions that were performed on the subjects over the 1.5-2 year lifespan of the animals. All imaging

was performed using a microPET/CT scanner (InveonTM dedicated PET docked with CT in the

multimodality platform, Siemens Medical Solutions, Malvern, PA). ^{18}F-flurodihydorotenol was used to

document the wall motion as it is taken up equally well in the SHR as well as normal controls. Imaging

issues at the 12-month acquisition resulted in unusable images at this time point. Data sets were named

70   by subject number and subject age (e.g. SHR2_20 refers the image acquistion done on SHR2 at the

subjects age of 20 months).

Prior to imaging, the animals were anesthetized with 2% isoflurane and oxygen. The animals

were then placed in the microPET scanner with ECG electrodes attached for gating. The animals were

injected via tail vein with 1-2 mCi of ^{18}F-flurodihydorotenol. Image acquisition began at the time of

75   injection. The microPET/CT system was used to acquire dynamic ECG-gated list mode PET data over

60 minutes. After the PET acquisition, a separate CT scan was acquired with 120 projections of continuous rotation to cover 220° with an x-ray tube operated at 80 kVp, 0.5 mA, and 200 ms exposure time. Listmode data were histogrammed into 8 gates of the cardiac cycle summed over the total acquisition after the initial few minutes for the studies documenting the wall mechanics. For the

80　dynamic and kinetic modeling studies, multiple gates of dynamic sequences, each of which consisted of complete tomographic projections, were histogrammed at 12 intervals of 5s, followed by 6 of 10s, 4 of 30s, 6 of 60s, and finally 10 intervals of 300s to give a total of 38 time frames over the 60 minutes. Dynamic sequences of 128×128×159 matrices of 0.776×0.776×0.796 mm^3 voxels were reconstructed using a 2D ordered-subsets expectation maximization [Fourier rebinning, OSEM (4 iteration and 16

85　subsets)] reconstruction algorithm supplied by the Inveon^{TM} imaging system software with attenuation correction using the x-ray CT images. No scatter correction was applied in this study.

Weight, LV Volume, and Wall Thickness Measurements

　　　Body weights were measured just prior to image acquisition for all SHR and WKY subjects. The

90　reconstructed ^{18}F-flurodihydorotenol images were used to determine LV lumen volumes at each gate of each image data set using Xeleris (Xeleris) software. The LV cavity volume data were used to calculate Stroke Volume (SV) and Ejection Fraction (EF). The LV cavity volume at the image gate corresponding to the reference state (see below) or reference configuration volume (ref vol) was also tracked over the lifespan, and was used as a measure of unloaded LV lumen volume. A potential correlation between

95　volume and EF was assessed.

　　　In order to document the extent of hypertrophy over time, one SHR and one WKY subject were sacrificed following the series of ^{18}F-flurodihydorotenol microPET image acquisitions performed at 6, 15, 18, and 20 months in order to measure the weight of the heart. Heart weight measurements were also made

8

of animals that died between image acquisitions. Hypertrophy was also documented with in vivo LV wall thickness measurements from the imaging data, using a mid-ventricle short axis slice of the reference image gate for each data set. Means and standard deviations of Body weight, SV, EF, ref volume, and wall thickness were calculated for each image acquisition time for the SHR and the WKY groups.

Strain Measurement by Hyperelastic Warping Image Registration

Hyperelastic Warping

Warping is an image registration technique that can provide estimates of the full 3D strain field of the LV directly from clinical imaging data. Complete details of warping theory and its application to nuclear imaging can be found in the following publications (Veress et al. 2005, Veress 2013, Veress 2005, Veress et al. 2008). Briefly, the technique uses the differences in image intensity between a template (reference) image data set and a target (deformed) image data set to deform a finite element (FE) representation of the template geometry into alignment with the target geometry, and thus obtains the deformation map between the two states (of the cardiac cycle) in the form of nodal strains (Veress 2013, Veress 2005). In this study, the registration solution evolved over seven intermediate images from early diastole (approximate stress-free state) through end systole. The image registration analysis was completed on a total of 33 image data sets.

Creation of Finite Element Models

An FE mesh was created for each image data set based on the geometry of the image gate approximately 1/3 of the way into diastole. This time point has been shown to be the closest to an unloaded state that occurs in-vivo (Kerckhoffs et al. 2009) and represents the reference state of the heart. The reference image gate was manually segmented, and the resulting closed contours were used to define the

9

FE mesh using TrueGrid preprocessing program (TrueGrid). Each FE mesh consisted of 15,448 nodes and 13,700 hexahedral (8-node solid) elements with B-bar (mean volumetric strain) formulation (Maker 1990).

125   The deformations assessed with warping are relatively insensitive to the material properties specified in the FE model (Veress et al. 2005). The passive constitutive model specified in this case was transversely isotropic hyperelastic, as is typically used in cardiac mechanics models. A description of the constitutive model and its FE implementation can be found in Weiss et al. (Weiss et al. 1996). Fiber inclination angles of -60, -30, 0, 25, 50 degrees (epicardium to the endocardium) were defined for each

130   model based on literature values (Hautemann 2007). Active fiber contraction was implemented following the approach used by Guccione and McCulloch (Guccione and McCulloch 1993) and further details can be found in Veress et al. (Veress et al. 2006).

Strain Data Analysis

135   The strain in the fiber direction is reported in this study because the goal was to estimate local elongation and shortening of the myocardial tissue during diastole and systole. The fiber strain, calculated as $\boldsymbol{a} \cdot \mathbf{E} \cdot \boldsymbol{a}$, where $\boldsymbol{a}$ is the fiber direction vector, and $\mathbf{E}$ is the Green-Lagrange strain tensor, was recorded at all of the nodes in the FE mesh for all image gates.

     Average fiber strain was calculated as the average of the nodal strain values in the whole LV mesh,

140   in order to obtain a measure of overall deformation. Average fiber strain was calculated at each of the 7 target image gates in the cardiac cycle with the average fiber strains at end-diastole (diastolic strain) and end-systole (systolic strain) being of particular interest. Differences between the SHR and WKY in diastolic strain and systolic strain were assessed at each image acquisition point over the lifespan of the subjects. Changes in diastolic strain and systolic strain between acquisition times were also assessed.

145   Regional fiber strains were also assessed for each image data set in order to determine whether functional changes occurred uniformly throughout the LV. Each model was divided into four regions (septal, anterior, lateral, posterior) using the attachment points of the right ventricle as anatomical landmarks. Regional average values of diastolic strain and systolic strain were determined for each image acquisition time, and regional differences were assessed. changes between acquisition times for regional

150   diastolic strain and systolic strain were also assessed.

Statistical significance of all differences in strain data between SHR and WKY, between acquisitions times, and between regions were assessed using the Student's t-test. Sample sizes were non-parametric. Statistical comparisons were considered significant at $p < 0.05$.

155

Comparison of Strain Data with Other Measurements

EF, volume, wall thickness, diastolic strain, and systolic strain were tabulated for each image data set in order to assess how changes in strain coincided with changes in geometry and hemodynamics. values of ef, ref volume, wall thickness, diastolic strain, and systolic strain were defined in order to separate the

160   data into those representative of "normal" states vs. those representative of "diseased" states. An ejection fraction value of EF < 0.45 (Aronow 2006, Fitzgibbons et al. 2009, Katz 2011, Kostis 2003, Midol-Monnet et al. 1987, Paulus et al. 2007, Wang and Nagueh 2009)(Bing et al. 1995) was used to define the diseased state. For systolic strain, diastolic strain, ref volume, and wall thickness, the mean and standard deviations of the WKY datasets were determined, then, the SHR data were given designations based on the number

165   of standard deviations the values were from the mean of the WKY data. This is intended to give an indication of the degree of abnormality of the SHR data.

11

RESULTS

170   **Weight, LV Volume, and Wall Thickness Measurements**

        The SHR showed progressive development of LV hypertrophy as evidenced by the changes in

both wall thickness measurements and heart-to-body weight ratio [Table 1]. LV wall thicknesses for the

SHR were similar to those of the WKY at 6 months, but the SHR subjects showed significant wall

thickening relative to the WKY controls at 15 months (p=0.003). The average SV remained relatively

175   constant over the lifespan for both groups [Table 2]. The average ref volume for the SHR increased

progressively from 12 to 20 months. Average EF for the SHR decreased to that being defined as low EF

at 18 months, and was below the low EF cutoff at the 20-month time point. A comparison between ref

volume and EF for individual subjects' data (rather than group averages) revealed a negative correlation

between rev volume and EF (R = -0.82).

180   **Table 1: Body weight (BW), Heart-to-body weight ratio (H/BW), Wall thickness. Values are means +/- standard deviation. "--" = data not available.**

	BW (g)	H/BW (mg/g)	Wall Thickness (mm)
6 months			
WKY	367.9 +/- 23.0 *(n=8)*	4.58 +/- 1.74 *(n=2)*	5.3 +/- 0.2 *(n=8)*
SHR	382.3 +/- 13.2 *(n=7)*	4.40 +/- -- *(n=1)*	5.2 +/- 0.1 *(n=7)*
12 months			
WKY	429.0 +/- 19.1 *(n=6)*	-- +/- --	-- +/- --
SHR	428.0 +/- 25.3 *(n=6)*	-- +/- --	5.6 +/- 0.7 *(n=2)*
15 months			
WKY	466.7 +/- 31.9 *(n=6)*	3.42 +/- -- *(n=1)*	5.4 +/- 0.4 *(n=6)*
SHR	433.0 +/- 36.0 *(n=6)*	4.62 +/- 0.30 *(n=4)*	6.2 +/- 0.2 *(n=4)*
18 months			
WKY	481.6 +/- 37.1 *(n=5)*	4.78 +/- -- *(n=1)*	5.5 +/- 0.4 *(n=4)*
SHR	415.0 +/- 24.0 *(n=2)*	6.54 +/- -- *(n=1)*	6.2 +/- 0.4 *(n=2)*
20 months			
WKY	487.0 +/- 29.0 *(n=4)*	3.42 +/- 0.44 *(n=3)*	5.2 +/- 0.1 *(n=4)*
SHR	384.0 +/- -- *(n=1)*	8.60 +/- -- *(n=1)*	6.6 +/- --

Table 2: Reference configuration volume, Stroke volume (SV), Ejection fraction (EF). Values are means +/- standard deviation. "--" = data not available.

	Ref Volume (mm³)	SV (mm³)	EF
6 months			
WKY *(n=8)*	208.6 +/- 33.9	337 +/- 68.2	0.68 +/- 0.05
SHR *(n=7)*	253.8 +/- 22.2	275 +/- 26.9	0.56 +/- 0.04
12 months			
WKY *(n=2)*	441.5 +/- 218.3	431 +/- 210.7	0.63 +/- 0.02
SHR *(n=2)*	222.1 +/- 23.0	309 +/- 53.6	0.60 +/- 0.04
15 months			
WKY *(n=6)*	232 +/- 55.6	363 +/- 63.2	0.67 +/- 0.04
SHR *(n=4)*	319.6 +/- 77.2	294 +/- 67.7	0.52 +/- 0.11
18 months			
WKY *(n=4)*	232.9 +/- 101.2	391 +/- 141.2	0.70 +/- 0.03
SHR *(n=2)*	471.3 +/- 329.4	284 +/- 103.4	0.46 +/- 0.28
20 months			
WKY *(n=4)*	218 +/- 42.7	335 +/- 24.4	0.71 +/- 0.09
SHR *(n=1)*	465.9 +/- --	222 +/- --	0.34 +/- --

Strain Measurement by Hyperelastic Warping Image Registration

The average strain in the LV over the cardiac cycle for each data set indicated a general trend in which the WKY controls show relatively unchanged deformation behavior over the lifespan, while the SHR subjects showed progressive decreases in diastolic and systolic strains over time [Figure 1].
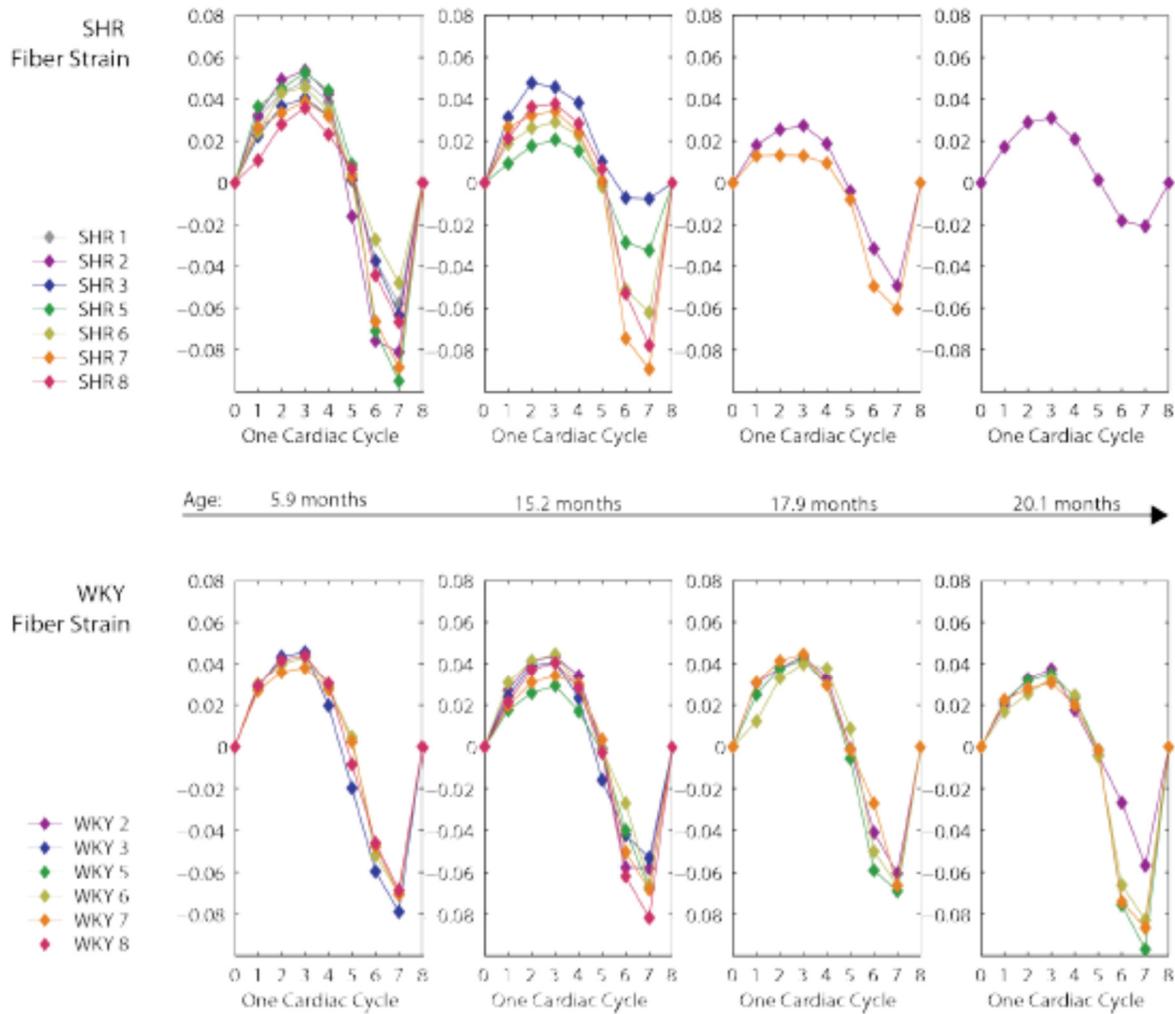
Figure 1   Fiber strain over the cardiac cycle for each individual data set. Results are grouped by type (SHR upper row, WKY lower row), and image acquisition time (left to right over the lifespan).

Significant differences between average SHR and WKY strain data were observed at the 18 month and 20 month image acquisitions [Table 3]. At 18 months, the SHR diastolic strain was significantly lower than the WKY controls ($p=0.009$). At 20 months, the systolic strain in the SHR subjects was significantly ($p=0.05$) less in absolute value than the WKY controls. More variability (larger standard deviations) in both diastolic strain and systolic strain were observed in the SHR data compared with the WKY data.

14

Table 3: Average end-diastolic fiber strain (diastolic strain) and end-systolic fiber strain (systolic strain). Strain data is averaged for all datasets at a given image acquisition time. Values are means +/- standard deviation. NS = not significant.

	Diastolic strain	Systolic strain
6 months		
WKY *(n=4)*	0.044 +/- 0.004	-0.070 +/- 0.007
SHR *(n=7)*	0.045 +/- 0.007	-0.071 +/- 0.017
P value	NS	NS
15 months		
WKY *(n=6)*	0.039 +/- 0.006	-0.066 +/- 0.010
SHR *(n=5)*	0.037 +/- 0.007	-0.059 +/- 0.036
P value	NS	NS
18 months		
WKY *(n=4)*	0.046 +/- 0.009	-0.067 +/- 0.003
SHR *(n=2)*	0.020 +/- 0.010	-0.055 +/- 0.008
P value	0.009	NS
20 months		
WKY *(n=4)*	0.034 +/- 0.003	-0.081 +/- 0.017
SHR *(n=1)*	0.031 +/- NA	-0.021 +/- NA
P value	NS	0.05

Evaluating the change in SHR strains between the 6-month image acquisition and later time points indicated that the deviation from normal diastolic strain occurred before similar changes in systolic strain. There was a significant decrease in diastolic strain between 6 and 18 months (p=0.004), and a significant decrease in systolic strain between 6 and 20 months (p=0.032).

The regional strain data for both the WKY and the SHR showed that the lateral region tended to have the greatest absolute value of mean diastolic strain and systolic strain [Figure 2]. For the WKY, the difference between the highest and lowest regional strains was much greater for systolic strain than for diastolic strain, indicating that normal LV function was characterized by greater regional differences in systole than in diastole. However for the SHR, the difference between the highest and lowest regional

strains was only slightly greater for systolic strain than for diastolic strain (less difference than was observed in the WKY).

220
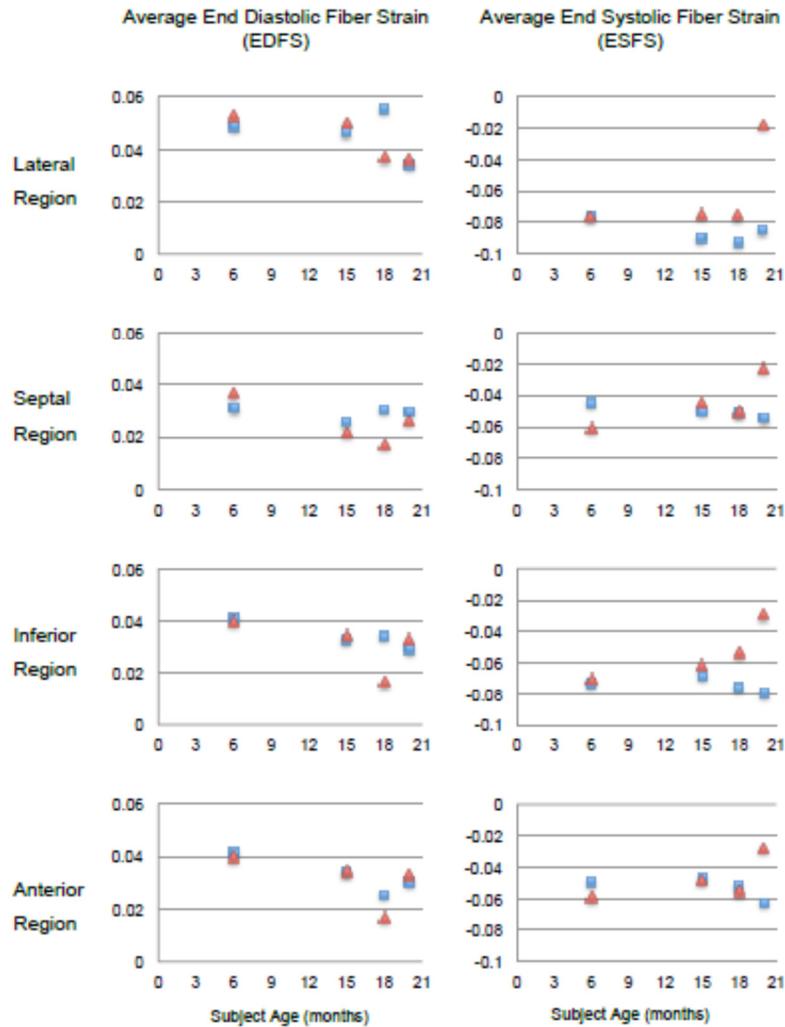
Figure 2   Regional diastolic strain (Left Column) and regional systolic strain (Right Column) vs. image acquisition time (subject age). Rows correspond to Lateral, Septal, Inferior and Anterior Regions. Triangles = SHR, Squares = WKY.

The SHR diastolic strain decreased for all regions between 6 and 15 months, and again between 15 and 18 months. The SHR systolic strain decreased for all regions between 18 and 20 months. The

largest difference between consecutive regional strains for the SHR occurred in the lateral region between 18 and 20 months. This suggests that heart failure in the SHR2 subject appeared to involve decreased systolic function in the lateral region of the LV, however, due to there being only a single subject severely limits the conclusions that may be drawn.

Comparison of Strain Data with Other Measurements

The SHR showed differences from the WKY in all measurements of LV structure and function. The EF, ref volume, wall thickness, diastolic strain and systolic strain results showed at least one SHR data set with a 3-sigma difference from normal function, with many 2-sigma and 1-sigma differences being observed [Table 4]. The primary results of the data comparison were:

(1) All image data sets with decreased diastolic strain showed LV hypertrophy, and the degree of decrease in diastolic strain appeared to match the degree of hypertrophy. The one case of 3-sigma decreased diastolic strain (SHR7_4) had 3-sigma increased wall thickness, and all of the 2-sigma and 1-sigma decreased diastolic strain cases also had 1-sigma or 2-sigma increased wall thickness.

(2) Subjects with severely decreased systolic strain had low or nearly low EF, but not all subjects with low EF had decreased systolic strain. The two data sets with 3-sigma decreased systolic strain had low or nearly low EF. However, there was one data set with low EF (SHR6_3) that did not have a low systolic strain.

(3) Hypertrophy was associated with other evidence of disease. Congestive heart failure with fluid in the lungs was observed at the time of death in the same three data sets (SHR3_3, SHR7_4, and SHR2_5) that had 3-sigma increased wall thickness.

Table 4: Ejection Fraction (EF), Reference Configuration Volume, Wall Thickness, End-Diastolic Fiber Strain (diastolic strain), End-Systolic Fiber Strain (systolic strain), Presence of congestive heart failure (CHF) for each individual SHR data set. ◆indicates EF<0.5. *, **, * indicate 1-sigma, 2-sigma, 3-sigma difference from "normal" values. + or – indicates presence or absence of CHF.**

SHR Subject	EF	Ref Volume (mm³)	Wall Thickness (mm)	Diastolic Strain	Systolic Strain	CHF
SHR1_1	0.58	271	5.2	0.049	-0.058 *	-
SHR2_1	0.58	222	5.2	0.054	-0.081	-
SHR2_4	0.66	238	5.9 *	0.027 **	-0.049 **	-
SHR2_5	0.34 ◆	466 **	6.6 ***	0.031 *	-0.021 ***	+
SHR3_1	0.58	238	5.1	0.041	-0.063	-
SHR3_3	0.47	423 *	6.6 ***	0.046	-0.008 ***	+
SHR5_1	0.59	260	5.3	0.053	-0.095	-
SHR6_1	0.55	238	5.1	0.046	-0.048 **	-
SHR6_3	0.39 ◆	330	6.0 **	0.029 *	-0.062	-
SHR7_1	0.58	260	5.3	0.039	-0.088	-
SHR7_3	0.61	282	6.1 **	0.034 *	-0.089	-
SHR7_4	0.26 ◆	704 ***	6.5 ***	0.013 ***	-0.060 *	+
SHR8_1	0.47	287	5.0	0.036	-0.067	-
SHR8_3	0.60	244	6.2 **	0.038	-0.078	-

255

DISCUSSION

Weight, LV Volume, and Wall Thickness Measurements

The time course of the development of myocardial hypertrophy in this study is consistent with the literature on the SHR when considering heart-to-body weight ratios (Bing et al. 2002), as well as wall thickness (Pfeffer et al. 1979). The relatively unchanging SV and noticeably decreasing EF in the aging SHR is consistent with previously reported results (Pfeffer et al. 1979). The relatively unchanging ref volume over much of the lifespan followed by an increase at the end of life is consistent with the literature suggesting that hypertension causes stable concentric hypertrophy over a long period of time followed by decompensation (Katz 2011). The proportionality between ref volume and EF suggests that LV lumen volume increase tends to coincide with failing pump function during the late stages of life in the SHR.

Strain Estimation by Hyperelastic Warping Image Registration

The observation of decreases in diastolic strain before decreases in systolic strain suggests that stiffening of the heart wall, associated with decreased diastolic filling, may precede the changes in systolic function that ultimately lead to heart failure. Increased stiffness of the myocardium may actually contribute to causing systolic contractile dysfunction by increasing the workload on the LV. This interpretation of the time course of changes involved in the development of hypertension induced hypertrophy is consistent with that reported previously (Katz 2011), however, this is the first study to quantify the separate time courses of changes in diastolic and systolic strain.

The regional strain data showed that the lateral region tended to have the greatest strains, in both diastole and systole, for both WKY and SHR groups. This result is intuitive because the lateral wall is the least constrained by the RV. Spatial differences in strain were greater in systole than diastole for both WKY and SHR. However, spatial differences in systolic strain was much less pronounced in the aging

19

280 SHR than in the WKY, indicating that the aging SHR may have pattern of altered LV mechanics in which the lateral region shows decreased systolic function. While the notion that pressure overload causes a relatively uniform change in passive material properties of the myocardium is well supported in the literature (Bing et al. 2002, Brooks et al. 2010), spatial variation in contractile function is not yet well understood because previous studies of strain have not separated diastolic and systolic effects. Further

285 research that assesses diastolic and systolic strains separately will be needed to address the question of spatial differences in systolic dysfunction.

Comparison of Strain Data with Other Measurements

The relationship observed between the degree of wall thickness increase and the degree of

290 reduction in diastolic strain suggests that hypertrophic adaptation reduces the LV's ability to stretch in diastole. It is generally understood that prolonged hypertension causes thickening and stiffening of the myocardium, which initially serves a compensatory role in response to pressure overload, but which ultimately contributes to HF when the LV becomes too stiff to allow for adequate filling volumes.

There was no direct relationship between EF and any strain measure because EF is a measure of

295 blood volume output, whereas strain is a measure of local tissue deformation relative to an intermediate reference configuration. A decreased EF can occur as a result of either decreased diastolic filling (low diastolic strain) or decreased systolic contraction (low systolic strain).

Limitations

300 A limited number of SHR data sets were present at the later stages of life because fewer of them lived until the end of the study. Future work will address this limitation by using a larger number of subjects. MicroPET imaging has a lower spatial resolution than some other imaging modalities. Improved

image resolution would result in greater accuracy of image-based strains. Blood pressure (BP) measurements were not made in this study due to experimental difficulties with the tail cuff method. Left ventricular pressure measurements via catheterization were intentionally not performed in this study because of the risks of infection and early death that often accompany repeated catheterizations (Bertrand 2011, Conti and Ross 1969, Midol-Monnet et al. 1987, Park et al. 2004). In future work, additional means of obtaining BP measurements will be pursued.

Conclusion

Image-based strain measurements that assess diastolic and systolic strains separately appear to be a promising means of gaining insight into the time course of hypertensive disease. By separating those effects, this study was able to document that reduced diastolic function (but not systolic function) is related to LV hypertrophy, and that spatial differences in systolic function (but not diastolic function) may play a role in the transition to heart failure in the SHR.

Disclaimer

This document was prepared as an account of work sponsored by the United States Government.

320   While this document is believed to contain correct information, neither the United States Government

nor any agency thereof, nor The Regents of the University of California, nor any of their employees,

makes any warranty, express or implied, or assumes any legal responsibility for the accuracy,

completeness, or usefulness of any information, apparatus, product, or process disclosed, or represents

that its use would not infringe privately owned rights. Reference herein to any specific commercial

325   product, process, or service by its trade name, trademark, manufacturer, or otherwise, does not

necessarily constitute or imply its endorsement, recommendation, or favoring by the United States

Government or any agency thereof, or The Regents of the University of California. The views and

opinions of authors expressed herein do not necessarily state or reflect those of the United States

Government or any agency thereof or The Regents of the University of California.

330

ACKNOWLEDGMENTS

340   **REFERENCES**

Aronow WS. 2006. Epidemiology, pathophysiology, prognosis, and treatment of systolic and diastolic heart failure. Cardiology in review. May-Jun;14:108-124.

Bertrand ME. 2011. What are the current risks of cardiac catheterization? Methodist DeBakey
345   cardiovascular journal. Jan-Mar;7:35-39.

Bing OH, Brooks WW, Robinson KG, Slawsky MT, Hayes JA, Litwin SE, Sen S, Conrad CH. 1995. The spontaneously hypertensive rat as a model of the transition from compensated left ventricular hypertrophy to failure. Journal of molecular and cellular cardiology.27:383-396.

Bing OH, Conrad CH, Boluyt MO, Robinson KG, Brooks WW. 2002. Studies of prevention, treatment
350   and mechanisms of heart failure in the aging spontaneously hypertensive rat. Heart failure reviews. Jan;7:71-88.

Brooks WW, Shen SS, Conrad CH, Goldstein RH, Bing OH. 2010. Transition from compensated hypertrophy to systolic heart failure in the spontaneously hypertensive rat: Structure, function, and transcript analysis. Genomics.95:84-92.

355   Conti CR, Ross RS. 1969. The risks of cardiac catheterization. American heart journal. Sep;78:289-291.

Costandi PN, McCulloch AD, Omens JH, Frank LR. 2007. High-resolution longitudinal MRI of the transition to heart failure. Magn Reson Med. Apr;57:714-720.

Feng L, Donnino R, Babb J, Axel L, Kim D. 2009. Numerical and in vivo validation of fast cine displacement-encoded with stimulated echoes (DENSE) MRI for quantification of regional cardiac
360   function. Magn Reson Med. Sep;62:682-690.

Fitzgibbons TP, Meyer TE, Aurigemma GP. 2009. Mortality in diastolic heart failure: an update. Cardiology in review. Mar-Apr;17:51-55.

Frohlich ED, Apstein C, Chobanian AV, Devereux RB, Dustan HP, Dzau V, Fauadtarazi F, Horan MJ, Marcus M, Massie B, et al. 1992. Medical Progress - the Heart in Hypertension. New Engl J Med. Oct
365   1;327:998-1008.

Guccione JM, McCulloch AD. 1993. Mechanics of active contraction in cardiac muscle: Part I--Constitutive relations for fiber stress that describe deactivation. Journal of biomechanical engineering. Feb;115:72-81.

Hautemann DJ. 2007. Fiber architecture of the post-mortem rat heart obtained with Diffusion Tensor
370   Imaging Eindhoven, Netherlands: Eindhoven University of Technology.

Hennersdorf MG, Strauer BE. 2007. The heart in hypertension. Internist. Mar;48:236.

Katz AM. 2011. Physiology of the heart. 5th ed. Philadelphia, PA: Wolters Kluwer Health/Lippincott Williams & Wilkins Health.

375   Kerckhoffs RC, McCulloch AD, Omens JH, Mulligan LJ. 2009. Effects of biventricular pacing and scar size in a computational model of the failing heart with left bundle branch block. Medical image analysis. Apr;13:362-369.

Kostis JB. 2003. From hypertension to heart failure: update on the management of systolic and diastolic dysfunction. American journal of hypertension. Sep;16:18S-22S.

380   Maker BN, Ferencz, R.M., Hallquist, J.O. . 1990. NIKE3D: A Nonlinear, Implicit, Three-dimensional Finite Element Code for Solid and Structural Mechanics. Lawrence Livermore National Laboratory Technical Report, UCRL-MA #105268.

Midol-Monnet M, Heimburger M, Davy M, Beslot F, Cohen Y. 1987. [Autonomic cardiovascular regulation and permanent catheterization in normotensive conscious (WKY) and spontaneously
385   hypertensive (SHR) rats]. Comptes rendus des seances de la Societe de biologie et de ses filiales.181:560-566.

Park P, Garton HJL, Kocan MJ, Thompson BG. 2004. Risk of infection with prolonged ventricular catheterization. Neurosurgery. Sep;55:594-599.

Paulus WJ, Flachskampf FA, Smiseth OA, Fraser AG. 2007. How to diagnose diastolic heart failure: a
390   consensus statement on the diagnosis of heart failure with normal left ventricular ejection fraction by the Heart Failure and Echocardiography Associations of the European Society of Cardiology: reply. Eur Heart J. Nov;28:2686-2687.

Pfeffer JM, Pfeffer MA, Fishbein MC, Frohlich ED. 1979. Cardiac function and morphology with aging in the spontaneously hypertensive rat. Am J Physiol. Oct;237:H461-468.

395   Phatak NS, Maas SA, Veress AI, Pack NA, Di Bella EV, Weiss JA. 2009. Strain measurement in the left ventricle during systole with deformable image registration. Medical image analysis. Apr;13:354-361.

Roger VL, Go AS, Lloyd-Jones DM, Benjamin EJ, Berry JD, Borden WB, Bravata DM, Dai S, Ford ES, Fox CS, et al. 2012. Heart disease and stroke statistics--2012 update: a report from the American Heart Association. Circulation. Jan 3;125:e2-e220.

400   TrueGrid [Livermore, CA: XYZ Scientific Applications, Inc. A Mesh Generator and Pre-Processor for FEA and CFD Analysis.] www.truegrid.com

Veress AI, Gullberg GT, Weiss JA. 2005. Measurement of strain in the left ventricle during diastole with cine-MRI and deformable image registration. Journal of biomechanical engineering. Dec;127:1195-1207.

405   Veress AI KG, and Gullberg GT. 2013. A Comparison of Hyperelastic Warping of PET Images with Tagged MRI for the Analysis of Cardiac Deformation. International Journal of Biomedical Imaging.2013.

Veress AI, Phatak, N., Weiss, J.A. 2005. Deformable image registration with Hyperelastic Warping In: Handbook of biomedical image analysis. New York: Marcel Dekker Inc.

410   Veress AI, Segars WP, Weiss JA, Tsui BM, Gullberg GT. 2006. Normal and pathological NCAT image and phantom data based on physiologically realistic left ventricle finite-element models. IEEE transactions on medical imaging. Dec;25:1604-1616.

Veress AI, Weiss JA, Huesman RH, Reutter BW, Taylor SE, Sitek A, Feng B, Yang Y, Gullberg GT. 2008. Measuring regional changes in the diastolic deformation of the left ventricle of SHR rats using
415   microPET technology and hyperelastic warping. Ann Biomed Eng. Jul;36:1104-1117.

Wang J, Nagueh SF. 2009. Current perspectives on cardiac function in patients with diastolic heart failure. Circulation. Mar 3;119:1146-1157.

Weiss JA, Maker BN, Govindjee S. 1996. Finite element implementation of incompressible, transversely isotropic hyperelasticity. Computer Methods in Applied Mechanics and
420   Engineering.135:107-128.

Xeleris [Arlington Heights, IL: MedX-Inc.] www.MedX-Inc.com